Modelling the Oscillating Pattern of the Apparent Spin Period of Inactive GLONASS Satellites

Nicola Cimmino
Astronomical Institute
University of Bern
Bern, Switzerland
nicola.cimmino@unibe.ch

Alessandro Vananti
Astronomical Institute
University of Bern
Bern, Switzerland
alessandro.vananti@unibe.ch

Thomas Schildknecht
Astronomical Institute
University of Bern
Bern, Switzerland
thomas.schildknecht@unibe.ch

***Abstract*—The spin period of a space debris is a key design parameter for Active Debris Removal missions. This parameter can be extracted from photometric data, in the form of light curves. The Astronomical Institute of the University of Bern has performed optical observations of inactive GLONASS satellites for more than eight years. The estimated spin period of a subset of these target satellites has shown two characteristics features: an oscillating pattern and a secular trend. This paper describes a simulation environment that allows modelling the long-term evolution of the spin period of a spacecraft, to understand which parameters affect the aforementioned features. Two simulated test cases are presented, demonstrating the capability of the model to capture these features, provided an ad-hoc set of initial parameters.**

Keywords—spin period, GLONASS, attitude evolution, active debris removal, box-wing satellite

I. Introduction

The increasing number of space debris in Earth's orbit has heightened the urgency for effective Active Debris Removal (ADR) strategies to maintain space sustainability [1]. A critical factor in ADR missions is understanding the spin period of target debris, as it significantly influences the approach and capture methodologies. ADR missions typically require a development time of 5 to 10 years from initial design to launch [2]. Within this timeframe, the spin period of space debris can evolve significantly. This evolution is driven by various factors, including environmental torques due to atmospheric drag, solar radiation pressure, Earth's gravitational field, and impact with other objects. Additionally, physical properties of the debris, such as its shape, mass distribution, and surface characteristics (e.g., specular or diffusive reflection), also play an important role in influencing the rate of spin change. To address this issue, it is crucial to not only determine the current spin period, but also to predict the long-term evolution of the angular speed.

Light curves, i.e., the time evolution of an object's brightness as seen from an optical sensor, are a widely utilized data source for retrieving a space object's spin period [3]. Current literature proposes several approaches to estimate the angular speed (or, similarly, the spin period) from light curves, depending on the observation time, data sampling frequency, presence of gaps in the data series, or whether data are unevenly spaced. Spectral analysis methods (e.g., Fast Fourier Transformation, FFT, Periodogram analysis, Welch's method) [4] estimate the power spectral density (PSD) of a signal, which reveals how the power of a signal is distributed over different frequency components. Each method involves transforming the time-domain signal into the frequency domain to identify dominant periodicities. While the FFT provides a direct computation of the signal's frequency spectrum, the periodogram offers an estimate of the PSD by computing the squared magnitude of the signal's Fourier transform. Welch's method enhances the periodogram approach by segmenting the data, applying window functions, and averaging the results to reduce variance in the PSD estimate. The main limitation of these approaches is that they assume that the data is evenly spaced in time. Other approaches have been developed to tackle this flaw. Epoch folding [5] aligns light curve data over a range of trial periods, folding the data to assess periodicity by minimizing scatter in the folded light curve. The Lomb-Scargle periodogram (LSP) [6], [7] is designed for unevenly spaced observations, estimating the power spectral density to detect significant periodic signals. Phase reconstruction methods [4] involve reconstructing the phase space of the light curve to identify periodicities, embedding the time series data into a higher-dimensional space to detect patterns corresponding to the spin period.

The Astronomical Institute of the University of Bern (AIUB) has a wide experience in acquiring and processing light curves. The observation facility of the AIUB is located in Zimmerwald, 10 km south of Bern (Switzerland). Here, photometric data have been acquired with the 1-m Zimmerwald Laser and Astrometry Telescope (ZIMLAT) and the 0.2-m Zimmerwald Small Aperture Robotic Telescope (ZimSMART) [8]. From the light curves measured in Zimmerwald Observatory, apparent rotational periods and their evolution have been estimated for various types of objects (e.g., box-wing spacecraft, upper stages, fragmentation pieces) at different orbital regimes. From 2015 to 2023, AIUB was in particular observing the Russian Global Navigation Satellite System (GNSS), GLONASS, since the Center for Orbit Determination in Europe (CODE) identified 70 decommissioned GLONASS satellites. Observed data of some of the GLONASS satellites show a periodic variability of the spin period and a secular (increasing/decreasing) trend. Understanding the factors impacting on such a trend is important to predict the time evolution of the spin period of inactive satellites and other space debris to support ADR mission design. Preliminary analyses have already been carried out at AIUB [4], [9], [10]. In particular, Rachman et al. [10] have performed statistical analyses on the observed GLONASS population, providing information on the average spin period, average cycle period, and secular trend. They also developed empirical models to fit observed data and extract future spin periods of GLONASS satellites. Moreover, a preliminary study on the dependencies of the spin period time evolution to solar panels configuration and surface properties has been performed.

This paper provides a brief overview of the observation campaign of inactive GLONASS satellites which were performed at Zimmerwald observatory from 2015 to 2023, and of the methodologies then adopted to extract the apparent spin period from light curves. Moreover, it describes a simulation environment to further understand which factors induce the oscillating pattern of the apparent spin period and its secular trend. To this aim, an open-source numerical propagator, namely Debris Spin/Orbit Simulation Environment (D-SPOSE) [11], has been used. D-SPOSE allows for coupled orbital and attitude propagation, provided a meshed model of the space object, surface properties and initial state conditions.

The remainder of the paper is organized as follows. Section 2 briefly describes the procedure to extract the spin period from light curves at AIUB and provides observational data of inactive GLONASS satellites. Section 3 describes the simulation environment, recalling the main physics forces and torques acting on Medium Earth Orbit (MEO) satellites. Section 4 presents some numerical results. In Section 5 conclusions and possible future works are discussed.

II. Spin Period Estimation From Light Curves

This section describes the procedure used at AIUB to estimate the apparent spin period of space objects from light curves as of January 2025.

The ZIMLAT telescope is a Ritchey-Chrétien telescope mounted on an alt-azimuth platform. It features a 1-meter aperture and a focal length of 4 meters. It is equipped with a 2048 × 2048 pixel CCD camera, offering a field of view (FoV) of 25.8' × 25.8'. For telescope pointing during observations, publicly available Two-Line Elements (TLEs) [12] are utilized in conjunction with the Simplified General Perturbations (SGP) model, as described in [13]. Data acquisition is performed in object tracking mode, as illustrated in Fig. 1 for the satellite GLONASS COSMOS 2380 (1995-009B). To enhance light curve sampling, the frame rate is increased by acquiring subframes of 200 × 200 pixels, as indicated by the grey square in Fig. 1 [3]. This approach achieves frame rates ranging from 1.0 to 0.17 frames per second. Each subframe is processed individually. An automated procedure measures the centroid of the object in the subframe and extracts its total intensity. By combining this data with time stamps from each frame header, a light curve is constructed, depicting relative intensity over time. During this process, most outliers, such as bright stars passing near the object, are removed. The resulting light curve, in the form of non-calibrated intensities, serves as the final product for further analysis.

Once extracted, the light curve undergoes manual preprocessing to identify any repeating patterns associated with the object's rotation. If such a pattern is detected, the light curve is further refined by eliminating residual outliers and trends, which can be caused by changes in the mutual geometry between the object and the observer, such as variations in phase angle. Based on the light curve's shape, three apparent attitude motion types are distinguished for an object. If no pattern related to the object's rotation is evident, the object is classified as *stable*. In cases where a dominant pattern is present but lacks visible repetition, the object is referred to as a *slow rotator*, indicating that the apparent (synodic) rotation period (P_a) exceeds the light curve's duration, a scenario common in Low Earth Orbit (LEO). Finally, light curves exhibiting a periodic pattern undergo further processing to extract P_a, and the object is classified as a *rotator*. *Rotators* undergo a two-steps algorithm for period estimation. First, an initial guess of P_a is computed with a parametric method (i.e., FFT, LSP). These methods are constrained by the Nyquist sampling criterion and cannot be applied if $f_a = \frac{1}{P_a} > 0.5\, f_s$ with f_s being the data sampling frequency. Therefore, to obtain confirmed values for P_a, a phase-diagram reconstruction method and, optionally, the epoch folding technique [5] are applied.

A specific observation target at Zimmerwald has been a set of GLONASS satellites. GLONASS is Russia's global navigation satellite system, positioned in MEO as the second such system after the Global Positioning System (GPS). Over nearly four decades, GLONASS has evolved through multiple satellite generations, including GLONASS I (Blocks IIa, IIb, IIv), GLONASS-M, and GLONASS-K [14], [15]. The standard configuration of a GLONASS constellation comprises 24 operational satellites distributed evenly across three orbital planes, each separated by 120° in the equatorial plane. The constellation's orbital inclination of approximately 64.8° enhances visibility over higher latitudes, including the Russian Federation. The satellites maintain their orientation using a yaw-steering attitude control mode [16].

At AIUB, GLONASS satellites have been typically observed with 1-second exposure times. As of July 2023, the AIUB database contains over 1,800 light curves representing 70 GLONASS satellites, totalling more than 540 hours of observations with a median duration of 9.59 minutes per session. Analysis of these light curves indicates that approximately 83% exhibit patterns where rotation periods can be determined relatively easily, allowing for the construction of phase diagrams. About 3% of the light curves are classified as *stable*, 10% as *slow rotators*, and 4% remain unfinished due to complex attitude motions or other factors [17]. Rachman et al. [10] identified that 26 GLONASS satellites display an oscillating pattern in their spin period evolution, featuring characteristic triangular shapes. They also observed that the absolute value of the slope of these patterns is roughly constant. Fig. 2 shows the spin period time evolution for GLONASS satellite Cosmos 2109 (a) and Cosmos 2179 (b), both of them exhibiting a one-year periodic pattern and a secular decreasing/increasing trend. In both cases, most of observations were carried out from January 2016 to June 2017.

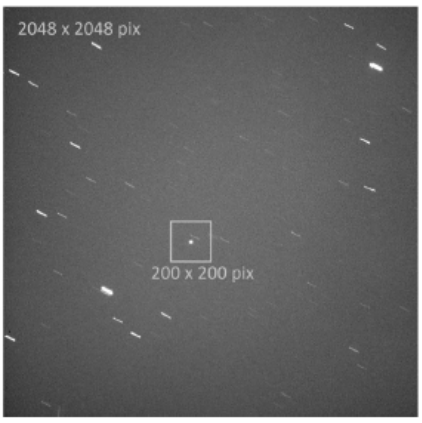

Fig. 1 - Full frame acquired by ZIMLAT telescope for satellite GLONASS COSMOS 2380 (1995-009B) during the object tracking mode. Used exposure time was 1.0 s. [3]

III. Simulation Environment

To model the long-term pattern of the spin period, an opensource software (D-SPOSE) has been adopted, which integrates three coupled differential equations. First, the dynamics equation for orbital motion in Earth-Centred Inertial frame:

$$\ddot{\boldsymbol{r}}(t) = -\frac{\mu}{r(t)^3}\boldsymbol{r}(t) + \sum_j \boldsymbol{a}_j(t, \boldsymbol{r}(t), \boldsymbol{v}(t), \boldsymbol{q}(t), \boldsymbol{\omega}(t)) \quad (1)$$

where $\boldsymbol{r}$ is the position as a function of time t, $r = \|\boldsymbol{r}\|$, $\boldsymbol{v}$ is the velocity, $\boldsymbol{q}$ is the attitude parametrization, chosen here to be a quaternion, $\boldsymbol{q} = [q_0\ \boldsymbol{q}_v^T]^T$, $\boldsymbol{\omega}$ is the angular velocity of the body with respect to the inertial frame, μ is the Earth's gravitational parameter, and $\boldsymbol{a}_j$ represents the additional considered accelerations due to orbital perturbations, which are a function of the rigid body's position, velocity, and attitude state.

Second, the attitude dynamics equation:

$$\boldsymbol{I}\dot{\boldsymbol{\omega}}(t) + \boldsymbol{\omega}(t)^{\times}\boldsymbol{I}\boldsymbol{\omega}(t) = \sum_j \boldsymbol{\tau}_j(t, \boldsymbol{r}(t), \boldsymbol{v}(t), \boldsymbol{q}(t), \boldsymbol{\omega}(t)) \quad (2)$$

where $\boldsymbol{\tau}_j$ represents the external torques, $\boldsymbol{I}$ is the matrix representation of the inertia tensor of the rigid body in the centroidal body-fixed frame. The superscript $\times$ denotes the skew-symmetric matrix representation of the cross-product.

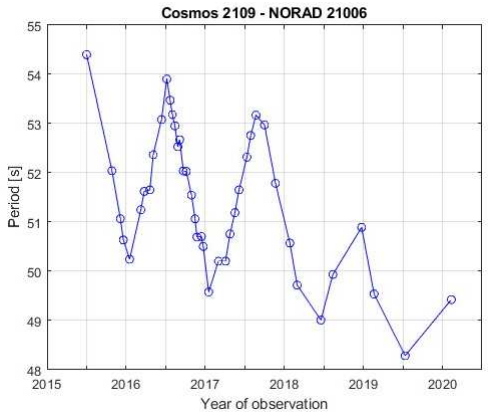

(a)

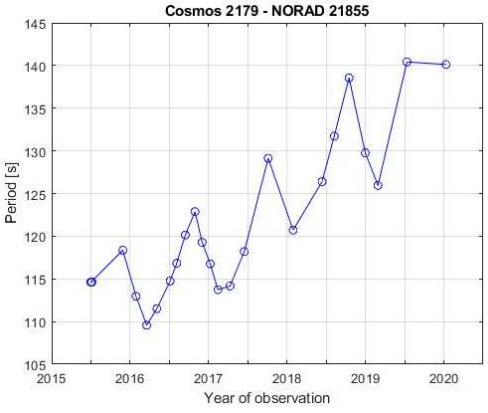

(b)

Fig. 2 – Apparent spin period of Cosmos 2109 (a) and Cosmos 2179 (b) observed at Zimmerwald observatory from 2015 to 2020.

Finally, the kinematic equation for the absolute orientation of the spacecraft:

$$\dot{\boldsymbol{q}}(t) = \frac{1}{2}\boldsymbol{\Omega}(\boldsymbol{\omega})\boldsymbol{q}(t) \quad (3)$$

where, being ω_x, ω_y and ω_z the angular velocity components in the body-frame:

$$\boldsymbol{\Omega} = \begin{bmatrix} 0 & -\omega_x & -\omega_y & -\omega_z \\ \omega_x & 0 & \omega_z & -\omega_y \\ \omega_y & -\omega_z & 0 & \omega_x \\ \omega_z & \omega_y & -\omega_x & 0 \end{bmatrix} \quad (4)$$

Eqs. (1)-(3) are numerically propagated at a fixed integration time step using the Runge-Kutta Dormand-Prince (RKDP) numerical integration method [18]. The same time step is used for propagating both the orbit and attitude equations as both are coupled.

The spin period (T) is then computed using the following equation:

$$T(t) = \frac{2\pi}{|\boldsymbol{\omega}(t)|} \quad (5)$$

Four input files are required to run the simulator:

- a TLE file corresponding to the initial epoch.
- a file containing the propagation parameters, among which the propagation time step and the propagation time.
- a file containing the model parameters (i.e., external perturbations). For the MEO regime, the following perturbations have been considered: asymmetry of the gravitational field (only J2), third-body (Sun and Moon), Solar Radiation Pressure (SRP), gravity gradient torque, and SRP torque. Moreover, the initial attitude of the spacecraft is described as a rotation of the Body Reference Frame (BRF) with respect to the Orbital Reference Frame (ORF) [13] with a classical (3-2-1)-sequence of Euler angles: yaw (ψ), pitch (θ) and roll (ϕ). Similarly, the initial angular velocity is expressed in terms of components of $\boldsymbol{\omega}$ in the BRF.
- a file containing information on the spacecraft geometry. Any spacecraft shape can easily be considered since the input consists of a list of triangular surfaces defined by the position of its three vertices in the body-fixed frame, the direction of its inward surface normal and the optical coefficients in the visible spectra. In particular, the surface properties are described by the coefficient of specular reflection (ρ), diffusive reflection (δ) and absorption (α). The three coefficients must satisfy the following constraint:

$$\rho + \delta + \alpha = 1 \quad (6)$$

IV. Results and Discussion

In a previous study [19], the authors have carried out a wide sensitivity analysis of the spin period time evolution for a generic box-wing satellite, located on a MEO orbit, varying the optical coefficients, the initial angular velocity, the initial

attitude state and the canting angle (β) of the solar panels, assuming the values reported in Table I. Moreover, an asymmetry of the canting angle has also been explored. Starting from the default configuration of β equal to 0°, the solar panels are canted of $\pm 5°$, $\pm 10°$ and $\pm 15°$.

In this work, a GLONASS I satellite has been used as reference for the simulation. The spacecraft has been modelled as a box-wing satellite with the following characteristics: a central box of size 4.0 × 2.0 × 2.0 m and two solar panels of size 0.0 × 3.5 × 4.0 m (see Fig. 3). The solar panels have an initial canting angle β equal to 0° with respect to the central box. The total mass of the satellite is 1400 kg [20] and the inertia matrix is:

$$\boldsymbol{I} = \begin{bmatrix} 1709.5 & 0 & 0 \\ 0 & 2305.3 & 0 \\ 0 & 0 & 2915.2 \end{bmatrix} kg\ m^2 \qquad (7)$$

The initial orbital parameters are extracted from the TLE of COSMOS 2109 (NORAD ID: 21006) at epoch 29th June 2015 16:29:34 UTC (see Table II).

Fixed the geometry and the mass distribution, two test cases are described. For both cases, the propagation time is 1825 days, and the integration step is 1 s. Starting from the outcomes of [19], the model parameters for the first test case (TC1) are the following:

- Canting angle, $\beta = \pm 5°$.
- Surface properties. Central box, +X face: ρ = 1.0; central box, -X, ± Y and ± Z faces: α = 1.0; solar panels, +X face: ρ = 0.35, δ = 0.35, α = 0.30; solar panels, -X face: δ = 1.0.
- Initial attitude state: (ψ, θ, ϕ) = [0, 0, 90] °.
- Initial angular velocity: $(\omega_x, \omega_y, \omega_z)$ = [0, 6, 0] °/s.

Fig. 4 shows the time evolution of the spin period using the parameters above. Two important features have been captured by the model and can be clearly noted in the figure: a yearly periodicity of T due to the yearly cycle of the Sun apparent motion around the Earth, and a decreasing secular trend (i.e., the spacecraft is spinning up). The former feature is attributable to the asymmetric canting angle, whereas the latter might be due to the asymmetry of the surface properties.

For the second test case (TC2), same canting angle, initial attitude state and initial angular velocity are set. The surface properties, instead, have been modelled as follows:

- Central box, ± X, ± Y and ± Z faces: α = 1; solar panels, +X face: ρ = 0.25, δ = 0.25, α = 0.50; solar panels, -X face: ρ = 0.50, δ = 0.25, α = 0.25.

In this case (Fig. 5) the spin period exhibits a yearly periodicity, as seen before, but an increasing secular trend (i.e., the spacecraft is slowing down). Also in this case, the two features can be attributable to the asymmetry of the canting angle and the asymmetry of the surface properties, respectively.

A few differences can be noticed when comparing observed and simulated data. The amplitude of the oscillations and the slope of the secular trend are larger in the simulated scenario. Moreover, observed data exhibit sharper variations of the spin period, with a characteristic "triangular" pattern. Such discrepancies can be attributable to the initial set of modelling parameters as well as to mismatches in the geometric and mass distribution properties of the modelled spacecraft.

TABLE I – MODEL PARAMETERS FOR THE SENSITIVITY ANALYSIS.

Parameters	**Values**
$\boldsymbol{\beta}$	{0, 45, 90, 135} °
α, δ, ρ	{0, 1}
ψ, θ, ϕ	{0, 90} °
$\omega_x, \omega_y, \omega_z$	{0, 3, 5} °/s

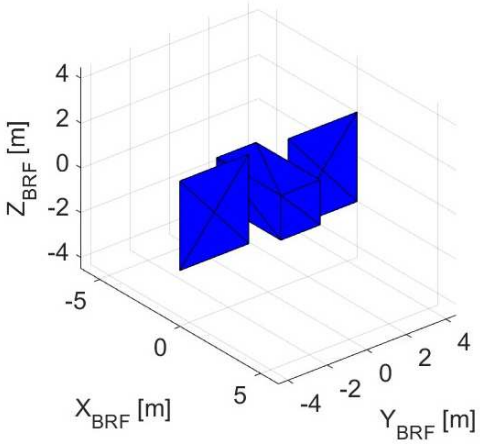

Fig. 3 - Meshed model of the spacecraft.

TABLE II - INITIAL ORBITAL PARAMETERS: SEMIMAJOR AXIS (*sma*), ECCENTRICITY (*ecc*), INCLINATION (*inc*), RIGHT ASCENSION OF ASCENDING NODE (*raan*), ARGUMENT OF PERIGEE (*aop*), TRUE ANOMALY (*ta*).

***sma* [km]**	***ecc* [-]**	***inc* [°]**	***raan* [°]**	***aop* [°]**	***ta* [°]**
25509.4	0.0082	64.1	208.8	186.2	339.0

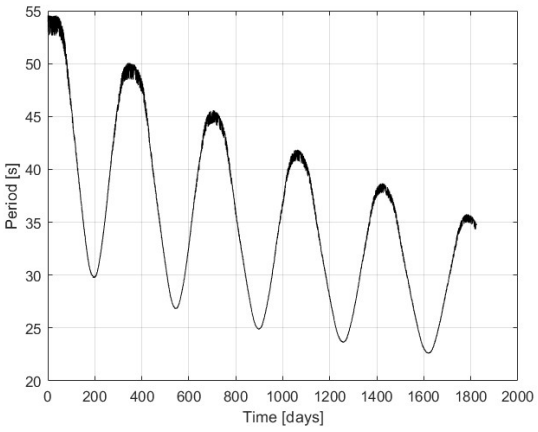

Fig. 4 – Modelled spin period for TC1.

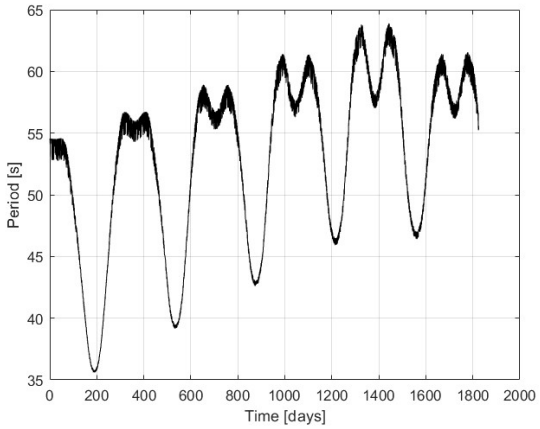

Fig. 5 – Modelled spin period for TC2.

V. CONCLUSIONS

This paper has provided a brief overview of the methodologies used at Zimmerwald observatory, from 2015 to 2023, to extract the apparent spin period of resident space objects from light curves. In particular, it has shown the long-term evolutions of P_a of two inactive GLONASS satellites, which feature an oscillating pattern and a secular trend. Moreover, a simulation environment has been described, which adopts an open-source software (i.e., D-SPOSE) to model the coupled orbital-attitude motion of any spacecraft, provided a meshed model of the geometry and its mass and surface properties. Two test cases have been presented, for which a simplified model of a GLONASS I satellite is generated. The configuration features an asymmetric canting angle of the solar panels of 5°. The two test cases differ for the surface properties of the spacecraft. The model has captured the 1-year periodic pattern of the spin period, as well as the decreasing/increasing secular trend. Further analyses should be carried out to reduce discrepancies between modelled and observed data. This includes further tuning of the initial attitude state and optical coefficients, as well as a higher fidelity model of the spacecraft geometry.

ACKNOWLEDGMENT

The authors would like to thank the Swiss National Science Foundation for providing the funds that supported the current study, and all the night observers and the technical staff at the Swiss Optical Ground Station and Geodynamics Observatory Zimmerwald.

REFERENCES

[1] ESA Space Debris Office, "ESA'S ANNUAL SPACE ENVIRONMENT REPORT," Darmstadt, Germany, Jul. 2024.

[2] A. E. White and H. G. Lewis, "An adaptive strategy for active debris removal," *Advances in Space Research*, vol. 53, no. 8, 2014, doi: 10.1016/j.asr.2014.01.021.

[3] J. Šilha, J. N. Pittet, M. Hamara, and T. Schildknecht, "Apparent rotation properties of space debris extracted from photometric measurements," *Advances in Space Research*, vol. 61, no. 3, 2018, doi: 10.1016/j.asr.2017.10.048.

[4] E. Linder, J. Silha, T. Schildknecht, and M. Hager, "Extraction of spin periods of space debris from optical light curves," in *Proceedings of the International Astronautical Congress, IAC*, 2015.

[5] S. Larsson, "Parameter estimation in epoch folding analysis," *Astron Astrophys Suppl Ser*, vol. 117, no. 1, 1996, doi: 10.1051/aas:1996150.

[6] M. Zechmeister and M. Kürster, "The generalised Lomb-Scargle periodogram," *Astron Astrophys*, vol. 496, no. 2, 2009, doi: 10.1051/0004-6361:200811296.

[7] G. Isoletta, R. Opromolla, and G. Fasano, "Attitude motion classification of resident space objects using light curve spectral analysis," *Advances in Space Research*, vol. 75, no. 1, pp. 1077–1095, Jan. 2025, doi: 10.1016/J.ASR.2024.10.034.

[8] J. Herzog, T. Schildknecht, A. Hinze, M. Ploner, and A. Vananti, "SPACE SURVEILLANCE OBSERVATIONS AT THE AIUB ZIMMERWALD OBSERVATORY," in *Sixth European Conference on Space Debris, Darmstadt, Germany*, 2013.

[9] A. Rachman, T. Schildknecht, and A. Vananti, "Analysis of temporal evolution of debris objects' rotation rates inside AIUB light curve database," in *Proceedings of the International Astronautical Congress, IAC*, 2018.

[10] A. Rachman, A. Vananti, and T. Schildknecht, "Spin Period Evolution of Decommissioned GLONASS Satellites," *Aerospace 2025, Vol. 12, Page 283*, vol. 12, no. 4, p. 283, Mar. 2025, doi: 10.3390/AEROSPACE12040283.

[11] L. B. M. Sagnières, I. Sharf, and F. Deleflie, "Simulation of long-term rotational dynamics of large space debris: A TOPEX/Poseidon case study," *Advances in Space Research*, vol. 65, no. 4, 2020, doi: 10.1016/j.asr.2019.11.021.

[12] "Space-Track.Org." [Online]. Available: https://www.space-track.org/auth/login

[13] D. Vallado and W. McClain, "Fundamentals of astrodynamics and applications, 2004," *Space Technology Library, Microcosm Press & Kluwer Academic Publishers*, 2007.

[14] B. Duan, U. Hugentobler, M. Hofacker, and I. Selmke, "Improving solar radiation pressure modeling for GLONASS satellites," *J Geod*, vol. 94, no. 8, 2020, doi: 10.1007/s00190-020-01400-9.

[15] G. Bury, K. Sośnica, R. Zajdel, and D. Strugarek, "GLONASS precise orbit determination with identification of malfunctioning spacecraft," *GPS Solutions*, vol. 26, no. 2, 2022, doi: 10.1007/s10291-021-01221-z.

[16] O. Montenbruck *et al.*, "GNSS satellite geometry and attitude models," *Advances in Space Research*, vol. 56, no. 6, 2015, doi: 10.1016/j.asr.2015.06.019.

[17] A. Rachman, "Understanding Attitude Behavior of Inactive GLONASS Satellites using Spin Period Evolution," Astronomical Institute University Bern , Bern, 2023.

[18] J. R. Dormand and P. J. Prince, “A family of embedded Runge-Kutta formulae,” *J Comput Appl Math*, vol. 6, no. 1, 1980, doi: 10.1016/0771-050X(80)90013-3.

[19] N. Cimmino, A. Vananti, and T. Schildknecht, “Predicting the Time Evolution of Space Debris Spin Period for Active Debris Removal Missions,” in *ESA Space Debris Conference*, 2025.

[20] S. Revnivykh, A. Bolkunov, A. Serdyukov, and O. Montenbruck, “GLONASS,” *Springer Handbooks*, pp. 219–245, 2017, doi: 10.1007/978-3-319-42928-1_8.